PNAS RESEARCH ARTICLE | CHEMISTRY

Synergistic material–microbe interface toward deeper anaerobic defluorination

Shun Che[a,b,1,2], Xun Guan[c,1,3], Roselyn Rodrigues[c,4], Yaochun Yu[a,b,5], Yongchao Xie[c], Chong Liu[c,d,6], and Yujie Men[a,b,6]

Edited by Thomas Mallouk, University of Pennsylvania, Philadelphia, PA; received January 9, 2024; accepted June 14, 2024

Per- and polyfluoroalkyl substances (PFAS), particularly the perfluorinated ones, are recalcitrant to biodegradation. By integrating an enrichment culture of reductive defluorination with biocompatible electrodes for the electrochemical process, a deeper defluorination of a C_6-perfluorinated unsaturated PFAS was achieved compared to the biological or electrochemical system alone. Two synergies in the bioelectrochemical system were identified: i) The in-series microbial-electrochemical defluorination and ii) the electrochemically enabled microbial defluorination of intermediates. These synergies at the material–microbe interfaces surpassed the limitation of microbial defluorination and further turned the biotransformation end products into less fluorinated products, which could be less toxic and more biodegradable in the environment. This material–microbe hybrid system brings opportunities in the bioremediation of PFAS driven by renewable electricity and warrants future research on mechanistic understanding of defluorinating and electroactive microorganisms at the material–microbe interface for system optimizations.

materials-microbe interfaces | per- and polyfluoroalkyl substances | defluorination

Significance

Given the incomplete and slow biodegradation of a limited number of per- and polyfluoroalkyl substances (PFAS), this work marks the endeavor combining PFAS-degrading microbial communities with state-of-the-art electroactive materials for enhanced bioremediation. The synergistic interactions between biological and electrochemical activities promoted defluorination in the bioelectrochemical system. These findings provide critical insights into the design and optimization of material–microbe hybrid systems for PFAS remediation.

Integrating electrochemically active materials with microorganisms offers a powerful strategy for creating hybrid biological-inorganic systems and enables many challenging chemical reactions with high efficiency and selectivity (1–5). By combining the unique reactivities from both electrochemistry and biochemistry, the material–microbe interface that benefits from synthetic and biological catalysts is proposed to yield reactivities that were initially difficult to achieve with either materials or microbes alone (4–7). We have demonstrated that such material–microbe interfaces are capable of fixing CO_2 and N_2 into chemicals, fuels, and fertilizers powered by either sunlight or electricity, with high efficiencies and reaction throughputs (8–12). These promising advances propel us to explore new applications and new reactivities with the utilization of material–microbe interface.

One potential application of the material–microbe interface for enhanced reactivity is the defluorination of per- and polyfluoroalkyl substances (PFAS). PFAS is a large family of over 10,000 manufactured chemicals (13), which have raised severe concerns for public health and ecosystems in recent decades due to their environmental persistence, widespread occurrence, and toxicity (14, 15). While the strong carbon-fluorine (C–F) bonds endow PFAS with extreme chemical and thermal stability for wide applications (16), the same property renders PFAS recalcitrant to environmental degradation, thus persistent in the environment and imposing adverse effects (17–19). It calls for innovative treatment technologies and remediation strategies for effective destruction via deep defluorination, where an appreciable number of C–F bonds in the molecule are broken with the release of fluoride (F^-) and the formation of less/nonfluorinated products. Less fluorinated products are typically more mobile, less bioaccumulative, and less persistent in the environment (20–22), hence deemed to be less toxic. Bioremediation, particularly with naturally occurring microorganisms under environmental conditions, is considered as a more cost-effective and sustainable option for pollutant degradation, including PFAS (23–25). However, such a bioremediation strategy is currently challenging due to its slow reaction kinetics and incapability of achieving deep defluorination and effective destruction.

Thus, we hypothesize that integrating defluorinating microorganisms with electrochemically active biocompatible materials would address the challenging degradation steps unachievable by microbes alone and lead to faster and more effective defluorination (Fig. 1*A*). This approach will not only retain the benefits of bioremediation but also offer improved PFAS defluorination performance. We further hypothesize that the potentially improved defluorination of such an integrated approach could be attributed to synergies from two aspects: i) the electrochemical effect, where the reductive electrochemical driving force on the electrode's surface offers additional electrochemical pathways of PFAS

Author affiliations: [a]Department of Chemical and Environmental Engineering, University of California Riverside, Riverside, CA 92521; [b]Department of Civil and Environmental Engineering, University of Illinois at Urbana-Champaign, Urbana, IL 61801; [c]Department of Chemistry and Biochemistry, University of California Los Angeles, Los Angeles, CA 90095; and [d]California NanoSystems Institute, University of California Los Angeles, Los Angeles, CA 90095

Author contributions: S.C., X.G., R.R., and Y.Y. performed research; S.C., X.G., R.R., Y.Y., Y.X., C.L., and Y.M. analyzed data; and S.C., X.G., C.L., and Y.M. wrote the paper.

The authors declare no competing interest.

This article is a PNAS Direct Submission.

[1]S.C. and X.G. contributed equally to this work.

[2]Present address: State Key Laboratory of Chemical Safety, China Petroleum and Chemical Corporation Research Institute of Safety Engineering Co., Ltd., Qingdao 266071, China.

[3]Present address: Department of Materials Science and Engineering, Stanford University, Stanford, CA 94305.

[4]Present address: Department of Chemistry and Biochemistry, College of Arts and Sciences, Gonzaga University, Spokane, WA 99258.

[5]Present address: Department of Environmental Chemistry, Swiss Federal Institute of Aquatic Science and Technology, Dübendorf CH-8600, Switzerland.

[6]To whom correspondence may be addressed. Email: chongliu@chem.ucla.edu or ymen@engr.ucr.edu.

This article contains supporting information online at https://www.pnas.org/lookup/suppl/doi:10.1073/pnas.2400525121/-/DCSupplemental.

Published July 23, 2024.

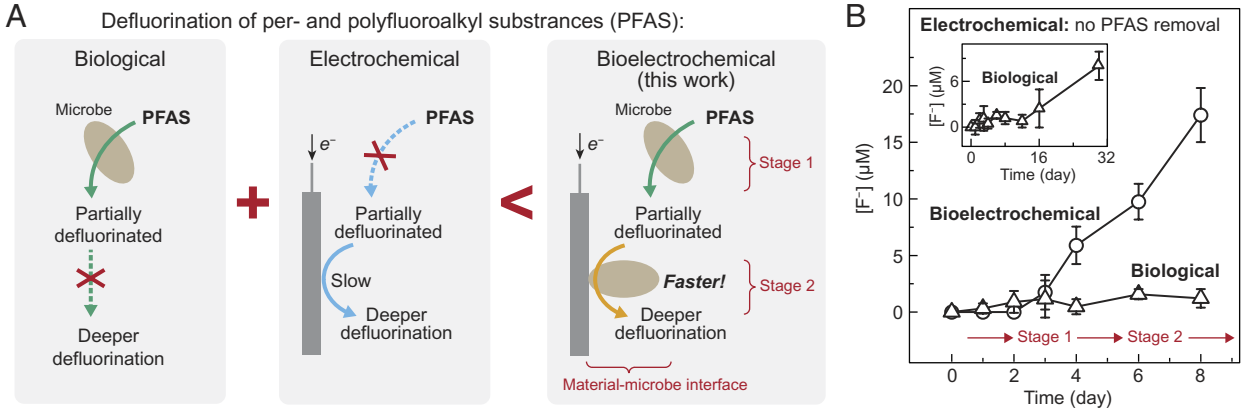

Fig. 1. Bioelectrochemical defluorination of PFMeUPA. (*A*) Scheme of the bioelectrochemical system. (*B*) Fluoride formation in the biological system (triangles) and the bioelectrochemical system (circles), the insert figure demonstrates fluoride formation in the biological system with extended incubation, $n = 3$, error bars represent SD.

decomposition and defluorination; ii) the bioelectrochemical effect, where the presence of electrochemical material–microbe interface may stimulate microbial processes (12, 26) or enable new microbial reactivities. The goal of this study was to test those hypotheses regarding the beneficial effects of the electrochemically driven material–microbe interface, which had not been experimentally demonstrated before.

Here, we report the faster and deeper PFAS defluorination thanks to the synergies identified at the electrochemical material–microbe interface. Neither the electrochemical nor the biological system alone could achieve the same performance. *E*-perfluoro (4-methylpent-2-enoic acid) (PFMeUPA) is one of the two perfluorinated structures reported to be reductively biodefluorinated by commonly available anaerobic microbial communities, and its biotransformation pathways have been elucidated (24, 27, 28). With PFMeUPA as a model PFAS molecule, we found that a hybrid system consisting of microbial consortium and biocompatible electrochemical cathode led to a faster release of F^- from the decomposition of PFMeUPA. Detailed characterization of the transformation products (TPs) during this process indicated the release of up to 6 F^- per PFMeUPA molecule, a much more significant extent of defluorination than the microbial approach with the release of 1 or 2 F^- per PFMeUPA (27). Moreover, the differences in TP formation between the electrochemical and bioelectrochemical systems implied that further defluorinating reactions forming less fluorinated products were enabled only at the material–microbe interface in the bioelectrochemical system. This proof-of-concept study demonstrates unique synergies between biocatalysis and electrochemistry that lead to faster and deeper defluorination and opens avenues of the material–microbe interface to treat challenging water pollutants, including PFAS and beyond.

Results

Faster and Deeper Defluorination in the Bioelectrochemical System. We integrated a PFMeUPA-defluorinating microbial community (27) with a previously developed biocompatible electrochemical system (8, 29) to investigate the defluorination performance. The defluorinating anaerobic microbial community originated from the dechlorinating microcosm KB-1 (27) and has been maintained with lactate and PFMeUPA for over 5 y (see details in the *Materials and Methods* section). The electrochemical system consisted of a cobalt–phosphorus (Co-P) cathode and a cobalt phosphate (CoPi) anode, and a constant voltage of −1.4 ± 0.19 V vs. Ag/AgCl was applied to the system for water electrolysis (Fig. 1*A* and *SI Appendix*, Fig. S1). In the absence of the defluorinating enrichment culture, the electrochemical system alone did not show defluorination or degradation of PFMeUPA (*SI Appendix*, Fig. S2). However, by inoculating the anaerobic PFMeUPA-defluorinating culture into the closed-circuit cathodic chamber, a fluoride formation of 17.4 ± 2.4 μM was achieved after 8 d. Such a defluorination performance is significantly higher than that in the biological system alone (1.2 ± 0.8 μM fluoride formation, Fig. 1*B*), where the same volume of the same culture was inoculated, amended with the same amount of PFMeUPA and with H_2/CO_2 as the headspace. In the biological system, the defluorination process did not start until a lag phase of 2 wk. It took more than 30 d to reach ~9 μM fluoride release (insertion of Fig. 1*B*), while the bioelectrochemical system doubled the fluoride release in half of the time.

We attributed the significantly higher and faster fluoride release in the bioelectrochemical system to synergistic effects at the material–microbe interface. There are two possible synergies involved in the bioelectrochemical system: i) in-series defluorination, i.e., the products of biological defluorination could be further defluorinated via abiotic electrochemical processes; ii) microbial defluorination processes could be enhanced at the cathodic electrode that holds the material–microbe interface. To demonstrate how each scenario contributed to the observed higher and faster defluorination in the bioelectrochemical system, we further introduced an abiotic electrochemical system inoculated with 5 mL cell-free spent medium of the same defluorinating enrichment culture as inoculated in the bioelectrochemical and biological systems. The spent medium was prepared by filtering a portion (~20 mL) of the same inoculation culture through a 0.22-μm filter. Thus, it was cell-free but contained the TPs of PFMeUPA in the defluorinating enrichment culture grown on lactate and with three doses of 70 μM PFMeUPA. The same bottle of culture was used for the inoculation of the three systems (i.e., 5 mL live culture for the bioelectrochemical and biological systems and 5 mL spent medium for the electrochemical system) for comparison. The same amount of PFMeUPA was amended in the three systems (Fig. 2*A*). By comparing the fluoride formation and analyzing the parent compound and TPs, we demonstrated the simultaneous occurrence of the two synergies between microbial and electrochemical processes in the bioelectrochemical system, which led to significantly higher and faster defluorination compared to the biological or electrochemical systems alone. In the following two sections, we described and interpreted the detailed results indicating that the two

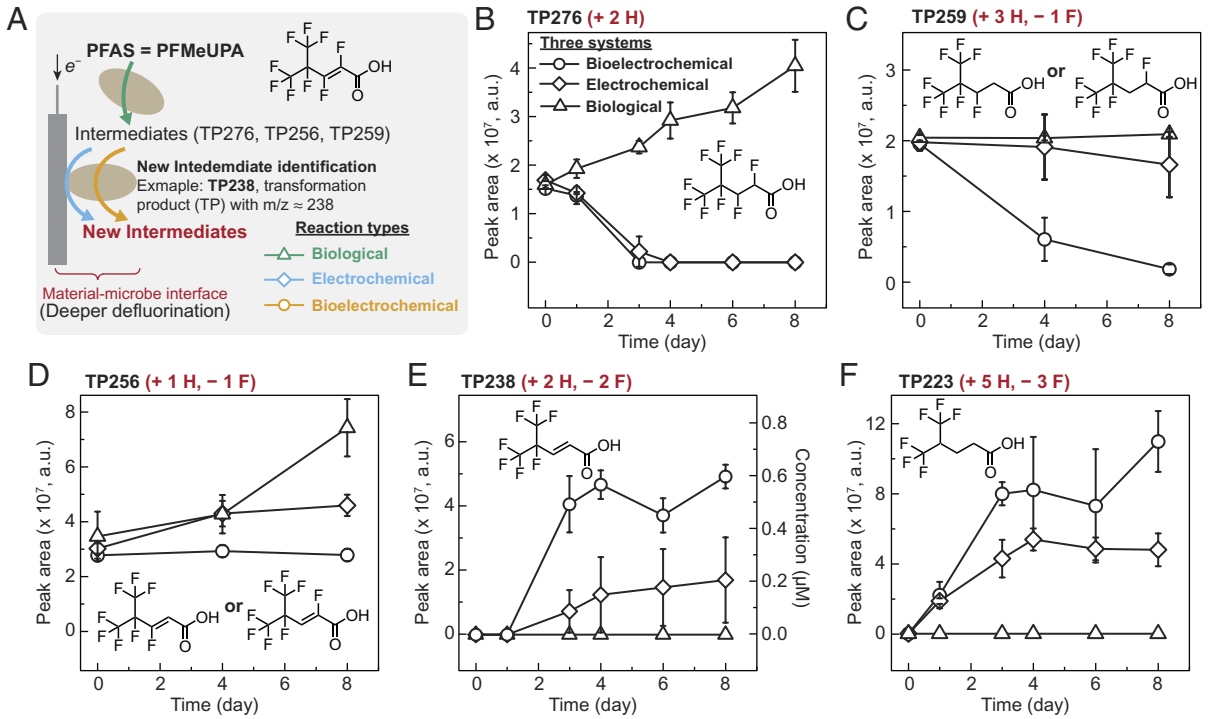

Fig. 2. Bioelectrochemical defluorination products of PFMeUPA. (*A*) Simplified defluorination pathway in the bioelectrochemical system. Arrows in green, blue, and yellow represent biological, electrochemical, and bioelectrochemical processes, respectively. (*B–F*) Formation of the major TPs, TP276, 259, 256, 238, and 223 (chromatographs, MS and MS2 spectra in *SI Appendix*, Fig. S4) in the biological, electrochemical, and bioelectrochemical systems. Biological system: triangles; Electrochemical system: diamonds; Biolectrochemical system: circles, $n = 3$, error bars represent SD. Note: despite no PFMeUPA addition or culture/spent medium inoculation in the anodic chamber, a slight diffusion of PFMeUPA and some TPs were observed in the anodic chamber. Thus, the total concentration or peak areas detected in both chambers were used in the plots.

proposed synergies were both observed at the electrochemically driven material–microbe interface.

Electrochemical Defluorination of PFMeUPA Biotransformation Products at the Material–Microbe Interface in the Bioelectrochemical System. We observed abiotic degradation of PFMeUPA biotransformation products via electrochemical processes. When the cell-free spent medium containing PFMeUPA biotransformation products (TP276, TP256, and TP259) was introduced into the electrochemical system containing newly spiked PFMeUPA (~70 μM), no removal of PFMeUPA was observed (*SI Appendix*, Fig. S3*A*) but with nonnegligible fluoride formation (*SI Appendix*, Fig. S3*B*). Such a fluoride formation could be attributed to the electrochemical defluorination of PFMeUPA biotransformation products carried over from the spent medium. This indicates the first proposed synergy of microbial-electrochemical in-series defluorination, where biotransformation products were further defluorinated by the abiotic electrochemical processes (the blue arrow in Fig. 2*A*). The microbial-electrochemical in-series defluorination contributed to the previously observed higher fluoride formation (Fig. 1*B*).

In the electrochemical system, one major carry-over biological end product, TP276 (via the biological hydrogenation of PFMeUPA) (27), was rapidly degraded (Fig. 2*B*), likely via the reductive defluorination forming TP259 and the HF elimination into TP256 (Figs. 2 *C* and *D* and 3*B*). TP259, another major end product of PFMeUPA biotransformation (via hydrogenation of the reductive defluorination intermediate TP256, -F+H+2H from PFMeUPA) (27), was further defluorinated via HF elimination (Fig. 2*C*) and resulted in a structurally confirmed intermediate of TP238 (Figs. 2*E* and 3*A*). Subsequently, several less fluorinated TPs were formed, likely from the further transformation of TP238 (Figs. 2*F* and 3*B*), suggesting deeper defluorination, i.e., more C–F bonds were cleaved per molecule. We confirmed the electrochemical defluorination of TP238 by spiking its reference standard into the same electrochemical system, and the same TPs (i.e., TP241, TP223, TP205, TP200, and TP169 in Fig. 3*B*) detected in the bioelectrochemical system spiked with PFMeUPA were formed from the electrochemical degradation of the standard compound of TP238 (*SI Appendix*, Fig. S5).

Overall, the major PFMeUPA biotransformation end products in the biological system can be further transformed and defluorinated via abiotic electrochemical processes in the bioelectrochemical system (Fig. 3*B*), demonstrating the synergistic effect via microbial-electrochemical in-series defluorination at the material–microbial interface. In the biological system, TP276 and TP259 were the two major end products from the anaerobic biotransformation of PFMeUPA. The integration of microorganisms with an electrochemical system surpasses the microbial limitation and breaks down those two biologically stable products into less fluorinated TPs, which could not be achieved by either biological or electrochemical systems alone.

Electrochemically Enhanced/Enabled Biotransformation Processes in the Bioelectrochemical System. Besides the synergy via microbial and electrochemical in-series defluorination, the second synergistic effect via electrochemically enhanced/enabled biotransformation was also observed in the bioelectrochemical system. Specific biotransformation processes were electrochemically enhanced, contributing to the deeper and faster defluorination of the parent compound. First, since the parent compound of PFMeUPA can only be transformed biologically (Fig. 2*A*), the observed faster removal of PFMeUPA in the bioelectrochemical system compared to others (*SI Appendix*, Fig. S3*A*) suggested an enhanced biotransformation of PFMeUPA. Similarly, the further biotransformation of TP256 was enhanced in the

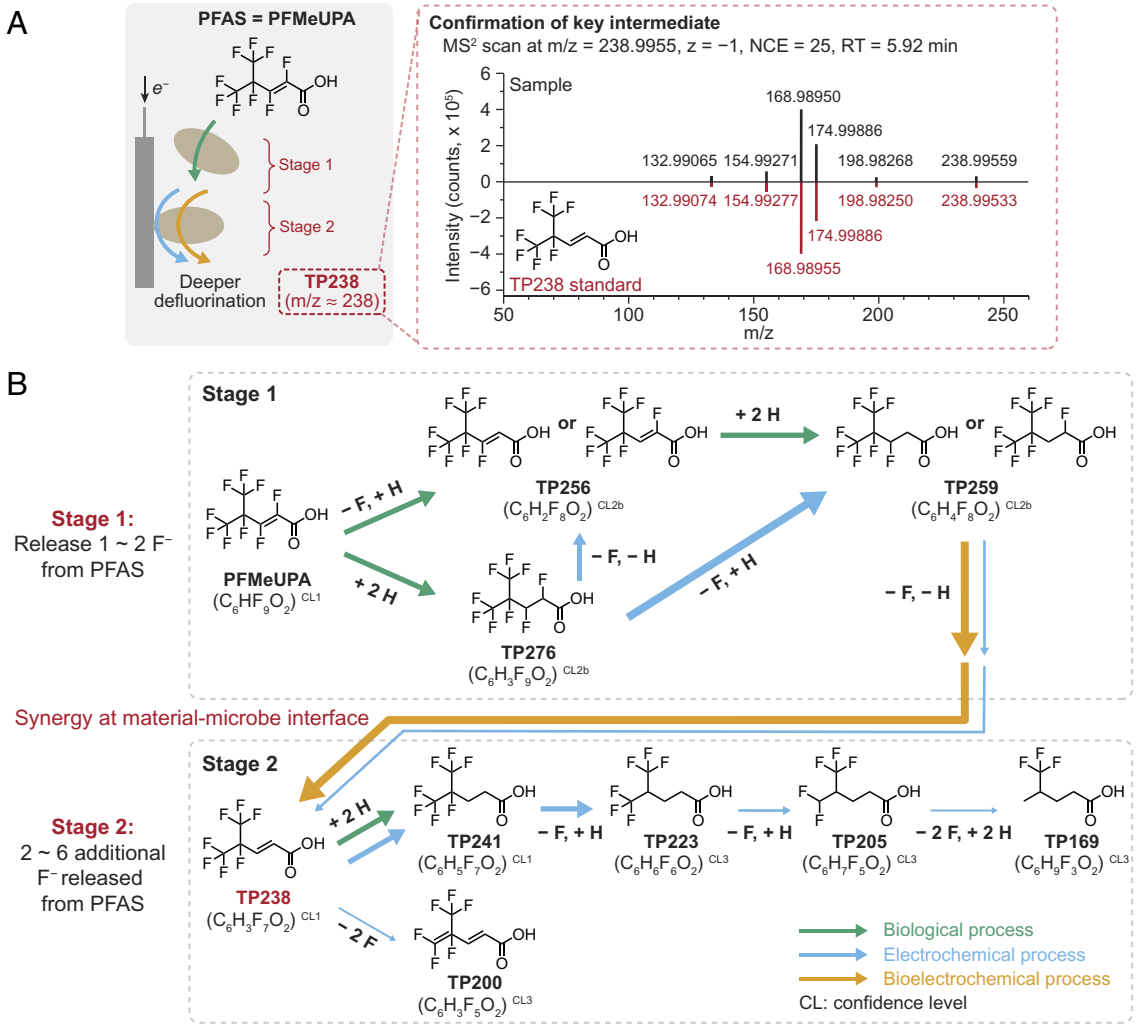

Fig. 3. PFMeUPA defluorination pathways at the material–microbe interfaces. (*A*) Validation of TP238 structure by comparing the retention times and MS^2 profiles between the experimental sample and the reference standard, 4,5,5,5-tetrafluoro-4-(trifluoromethyl)-2-pentenoic acid. (*B*) Proposed biotransformation pathways of PFMeUPA in the biological, electrochemical, and bioelectrochemical systems [all listed TPs were detected in at least one of the three systems; CL: confidence level of the identified TPs determined according to the criteria by Schymanski et al. (30); the thickness of arrows indicates the relative contributions of the reactions to the transformation; the text next to each arrow indicates the changes in formula from PFMeUPA; see *SI Appendix*, Fig. S6 regarding the formation curves of the deeper defluorination products, i.e., TP241, TP205, TP200, and TP169].

bioelectrochemical system since the level of TP256 was higher in the biological system compared to the bioelectrochemical system (Fig. 2*D*).

On top of the electrochemically enhanced microbial transformation of PFMeUPA, we also observed electrochemically enabled biodefluorination of some intermediates such as the HF elimination of TP259 to form TP238. TP238 cannot be formed from PFMeUPA by the biological system alone (27). Although the electrochemical system alone also converted TP259 into TP238 and subsequent TPs, the bioelectrochemical system achieved a much faster removal of TP259 (Fig. 2*C*), corresponding to the faster formation of TP238 (Fig. 2*E*). Thus, it indicated that electrochemically enabled biological processes substantially contributed to the transformation of TP259 to TP238, and such defluorination processes were unique in the bioelectrochemical system as the biological system was unable to further decompose TP259 (27).

According to a previous study, in the biological system spiked with TP238 standard compound, it was only transformed into the end product TP241 via hydrogenation without further degradation (27); however, in the bioelectrochemical system, TP241 was further transformed into less fluorinated TPs, i.e., TP223, TP205, TP200, and TP169 (Fig. 3*B* and *SI Appendix*, Fig. S6). All these downstream TPs could be formed from TP238 via electrochemical defluorination processes (*SI Appendix*, Fig. S5). Given that there were no significant differences in the formation of those TPs, except for TP223, between the bioelectrochemical and the electrochemical systems (*SI Appendix*, Fig. S6), it was most likely that the electrochemical defluorination played a major role in their formation in the PFMeUPA-spiked bioelectrochemical system. The higher level of TP223 in the bioelectrochemical system (Fig. 2*F*) was probably due to more TP238 formed (Fig. 2*E*) from the electrochemically enabled biodefluorination of TP259.

Shift of Community Structure at the Material–Microbe Interface of the Bioelectrochemical System. The electrochemically enhanced and enabled biological processes suggested that specific microbial groups were selected in the bioelectrochemical system. Therefore, we conducted the 16S rRNA gene amplicon sequencing to examine the changes in the composition of microbial communities in the bioelectrochemical system compared to the one in the biological system (Fig. 4*A*). Since the same cathode material was also added to the biological system, we divided the microbial community in the biological and bioelectrochemical systems into two groups: the one

in planktonic growth (i.e., entries 1 and 3 for the biological and the bioelectrochemical system, respectively) and the one attached to the cathode material (i.e., entries 2 and 4 for the biological and the bioelectrochemical system, respectively) (Fig. 4*A*). Differences in microbial compositions of those communities were examined using 16S rRNA gene amplicon sequencing.

We observed significant differences in microbial distributions and community compositions between the biological and bioelectrochemical systems. First, in the biological system, microorganisms were distributed both in suspension and on the cathode surface with similar community structures. Different from the biological system, in the bioelectrochemical system with the addition of electricity, microorganisms were prone to attach to the cathode materials, with only a small amount of genomic DNAs extracted from the cells collected from the culture suspension (i.e., only one out of the four replicates retrieved sufficient DNA for the sequencing analysis as shown in entry 3 in Fig. 4*B*). The planktonic community in the bioelectrochemical system (entry 3) also revealed a similar taxonomic distribution to the cathode-attached community (entry 4 in Fig. 4*B*). The similar compositions of the planktonic and surface-bound communities in the same system suggested that physical adsorption to the cathode material did not significantly alter community structures. Instead, the addition of electricity altered the space distribution of microorganisms by promoting cell attachment to the cathode. Second, we observed a substantial shift of community composition from the biological system after introducing electricity on the cathode, which was consistent with the results from scanning electron miscopy (*SI Appendix*, Fig. S8). A specific taxonomic group (TAXA1) in the genus *Clostridium* became dominant in the community bound to the electricity-applied cathode surface with an average relative abundance of 80% compared to 29% in the biological system without the electric circuit applied. Meanwhile, the most dominant taxonomic group in the biological system, TAXA2 (an unspecified *Clostridiales* family bacterium), was outcompeted to near extinction in the bioelectrochemical system. Although TAXA1 and TAXA2 were the closest among all abundant taxonomic groups, they only had 87.5% similarity of the 16S rRNA gene (Fig. 4*C*) and could be quite different in physiological characteristics and electroactive properties given their different responses to the addition of electricity.

Discussion

An electricity-driven material–microbe system uniquely achieved faster and deeper defluorination of PFMeUPA compared to the biological or electrochemical system alone, which were contributed by two types of synergies at the electrochemically driven microbial–material interface. First, the major stable products of PFMeUPA (i.e., TP276 and TP259) from biological processes were able to be further transformed via electrochemical processes, partially contributing to the formation of less fluorinated TPs, hence higher defluorination. Second, unique electrochemically enhanced and enabled biological processes contributed to the faster degradation of PFMeUPA as well as the higher formation of less fluorinated TPs (e.g., TP238 and TP223). Collectively, the two synergies elucidated in the as-demonstrated bioelectrochemical system together achieved up to six F^- released from each parent compound molecule, which is much higher than one F^- released in the biological system alone (27).

The TP analysis highlighted the unique electrochemically enabled biodefluorination reactions, such as the formation of TP238 from TP259 (one stable product in the biological system alone), which is a key step leading to further electrochemical defluorination. However, it is still unclear which microorganisms could benefit from the electrochemically active cathodic environment and obtain the new capability. The dominant *Clostridium* spp. in the microbial community of the bioelectrochemical system were likely the electroactive ones similar to those *Clostridium* species, *Clostridium cochlearium*, *Clostridium butyricum*, *Clostridium ljungdahlii*, and *Clostridium aceticum*, known to be electroactive in other bioelectrochemical systems (31–33). All reported PFAS biotransformation so far, including the aerobic transformation of polyfluorinated compounds and the reductive defluorination of the perfluorinated PFMeUPA, did not support cell growth (20–22, 24, 34–38). This makes it more challenging to identify the responsible ones by simply

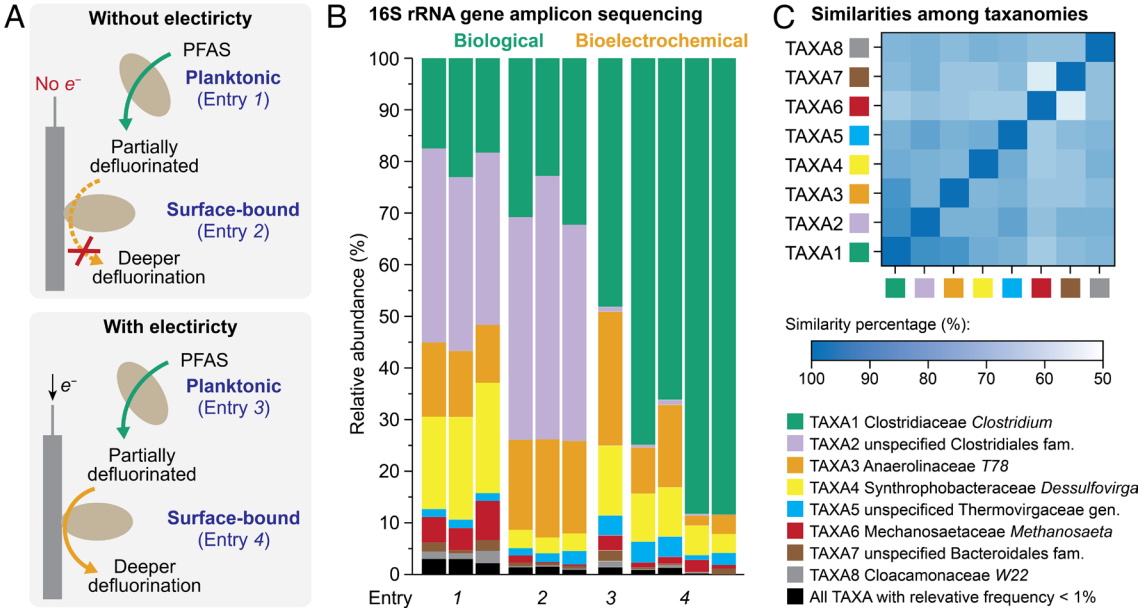

Fig. 4. Community shift in the bioelectrochemical system. (*A*) Sample entries investigated by the 16S rRNA gene amplicon sequencing; (*B*) The top eight taxa with >1% relative abundance according to the 16S rRNA gene amplicon sequencing analysis. The assigned taxonomic classification is listed as family name followed by genus name; (*C*) Similarity among the top eight taxa identified in the microbial communities (see the phylogenetic distribution of OTUs in the eight taxa in *SI Appendix*, Fig. S7).

comparing community differences between the biological and bioelectrochemical systems. Nonetheless, we may still reasonably infer that the dominant microbes attached to the cathode surface could be plausible candidates for screening in future studies. A recent report on certain acetogens capable of PFMeUPA reductive defluorination might also provide some insights into the future identification of the responsible microorganisms in the bioelectrochemical system (28). It is also worth noting that the transformation of PFMeUPA could only be realized by microbial processes. Thus, ensuring continuous biodegradation of PFMeUPA, in other words, sustained growth of the degrading microorganisms in the bioelectrochemical system, is pivotal. Despite the enhanced defluorination degree of PFMeUPA in the bioelectrochemical system, we observed slowed PFMeUPA degradation over time, suggesting a decrease in microbial activities. As the microorganisms capable of reductive defluorination are being identified and characterized (28), we point future directions toward optimizing the bioelectrochemical system by selecting and utilizing more efficient defluorinating microbial cultures and operating in their favorable growth conditions after a better understanding of the physiological and molecular characteristics of the defluorinating microbes.

The PFAS compound used in this proof-of-concept study represents an important group of PFAS (i.e., unsaturated ones), which have been synthesized as the building blocks and key intermediates in the organofluorine industry (15, 39–42). Compared to the biological system that only worked with per- and polyfluorinated unsaturated structures (24), the bioelectrochemical system enabled defluorination of a wider range of PFAS compounds with different structures, suggesting its transformative potential to be adapted to other PFAS compounds. Complete defluorination leading to benign products would be the ultimate treatment goal, but it is very challenging. In the current bioelectrochemical system, although the parent compound was not fully mineralized, the bioelectrochemically enhanced defluorination resulted in less fluorinated products, which tend to be less toxic and less persistent in the environment. Overall, the demonstrated bioelectrochemical system opens another route for degrading the notorious PFAS compounds with an extension of the slow and limited defluorination process in biological systems, casting light on future designs of defluorination systems with unique synergies at the material–microbial interface to enhance PFAS destruction.

Materials and Methods

Chemicals. Standard compounds of (E)-perfluoro(4-methylpent-2-enoic acid) (denoted "PFMeUPA" (27), CAS number:103229-89-6), and 4,5,5,5-tetrafluoro -4-(trifluoromethyl)-2- pentenoic acid (CAS number: 243139-64-2) were purchased from SynQuest Laboratories (Alachua, FL). A 10 mM stock solution of each standard was prepared in autoclaved anaerobic Milli-Q water in a 160-mL sealed serum bottle and stored at room temperature until use.

Cultures and Growth Conditions. The defluorinating enrichment originated from KB-1® generously provided by SiREM Lab (https://www.siremlab.com/) and has been maintained in Men's lab since 2017. The cultures for inoculation were maintained in 160-mL sealed serum bottles containing 100 mL of a sterile anaerobic basal medium buffered at pH 7.0 to 7.5 with 100 μg/L vitamin B_{12} and an Ar/CO_2 headspace (*SI Appendix*, Table S1) (43, 44). Lactate (20 mM) was added as the electron donor and the primary growth substrate. PFMeUPA (~70 μM) was added as the external electron acceptor and re-added upon depletion (indicated by ~70 μM fluoride formation) till three doses. All cultures were incubated at 34 °C in a dark incubator without shaking. The microbial viability was examined by measuring fluoride ion formation from the spiked PFMeUPA.

Electrode Plating. The CoPi and Co-P alloy electrodes were prepared by electrochemical deposition following the previously reported method (8). The electrochemical deposition was conducted in a three-electrode system with a working electrode of electrode substrate, a counter electrode of Pt wire (CH Instrument CHI115), and a reference electrode of Ag/AgCl (1 M KCl) (CH Instrument CHI111P) with the Gamry Interface 1000E potentiostat. The deposition solution of the CoPi electrode contains 10 mM $Co(NO_3)_2$ and 0.1 M methylphosphonate (MePi) buffer (pH 8). The carbon cloth (Fuel Cell Earth CC6P40), which was sequentially rinsed with acetone and DI water, was applied as electrode substrates. The deposition was performed at 0.85 V vs. reference until 500 mC/cm^2 charge was passed. The deposition solution of the CoP electrode contains 0.15 M H_3BO_3, 0.1 M NaCl, 0.33 M $Na_2H_2PO_2$, and 0.2 M $CoCl_2$. The stainless mesh (AlfaFisher 45002-CH), which was sequentially rinsed with acetone and DI water, was applied as electrode substrates. The deposition was performed at −1.2 V vs. reference for 15 min.

Bioelectrochemical System Setup. Experiments of bulk electrolysis were conducted in a custom-made two-chamber glass electrochemical cell (Adams and Chittenden Scientific Glass). It had two 150-mL chambers separated by a Nafion 117 membrane (Sigma-Aldrich 274674-1). The experiments were run in parallel using an eight-channel Gamry Interface 1000E potentiostat interfaced with a Gamry ECMB multiplexer. The incubation temperature was 30 °C, which was maintained by a water bath with constant stirring of 150 rpm under a pure N_2 gas atmosphere. The working electrode was a stainless-steel mesh electrodeposited with CoP alloy catalyst ("*Electrode Plating*"), the counter electrode was the carbon cloth electrodeposited with CoPi catalyst (*Electrode Plating*), and the reference electrode was the leak-free Ag/AgCl reference electrode (Innovative Instruments, Inc. LF-1-100). The cathodic chamber was flushed with pure N_2 gas, and then, 95 mL of modified BAV1 medium containing ~70 μM PFMeUPA was transferred anaerobically into the cathodic chamber. The reducing agent, sodium sulfide + L-cysteine (*SI Appendix*, Table S1), was added as needed to maintain the anaerobic condition. Then, in the triplicated bioelectrochemical system, 5 mL of 100 mL maintained inoculation culture (after three doses of PFMeUPA) was injected into the cathodic chamber to make the final electrolysis suspension/solution. The anodic chamber contained 100 mL of modified BAV1 medium only. Multiplexed chronoamperometry was performed on the reactors under the selected voltage to yield the targeted current densities (~1 mA/cm^2).

The electrochemical system was set up in triplicates in the same way as the bioelectrochemical system, except that 5 mL spent medium (0.22 μm filtrate of the same culture used for inoculating the bioelectrochemical system) was inoculated into the cathodic chamber instead of the living culture. The biological system was set up in triplicates by inoculating 5 mL of the same culture used for the bioelectrochemical system into 160 mL sealed serum bottles containing 95 mL of modified BAV1 medium (*SI Appendix*, Table S1). A pure H_2 headspace was used to mimic the headspace of the cathodic chamber in the bioelectrochemical system, and the same cathode material used in the bioelectrochemical system was added to the serum bottle. The addition of the cathode material in the biological system was to examine its effect on microbial activities and the microbes attached to it.

Two mL liquid from the cathodic and anodic chambers of the bioelectrochemical and electrochemical systems and the biological system was taken by syringes on days 0, 1, 2, 3, 4, 6, and 8. The samples were centrifugated at 13,000 rpm for 15 min at 4 °C. The supernatant was stored at 4 °C for F^-, parent compound, and TP analyses, while the cell pellets were kept at −20 °C for the 16S rRNA gene amplicon sequencing. At the end of the experiment, the cathode material in the bioelectrochemical and biological systems was taken out and stored at −20 °C for the 16S rRNA gene amplicon sequencing.

Potential adsorption of PFMeUPA and its TPs (i.e., TP276, TP256, and TP259) was tested (*SI Appendix*, *Supplemental Methods*), and no adsorption was observed. Fluoride and other anionic compounds were rejected by the cation-exchange membrane and not detected in the anodic chamber, except PFMeUPA, TP256, and TP259. A modified SPE protocol (*SI Appendix*, *Supplemental Methods*) was applied to extract those compounds from the anodic samples to remove the salts. Total peak areas of samples from both chambers were reported for those compounds.

Fluoride-Ion Measurement by the Ion-Selective Electrode Method. Fluoride ion was measured using an ion-selective electrode (ISE) (HACH). The detection limit was 0.02 mg/L (ca. 1 μM). The fluoride measurement by ISE was previously cross-validated using ion chromatography (27).

High-Performance Liquid Chromatography Coupled to High-Resolution Tandem Mass Spectrometry Analysis. The parent PFAS compounds and TPs were analyzed by an Ultrahigh performance liquid chromatography coupled to

a high-resolution quadrupole orbitrap mass spectrometer (UHPLC-HRMS/MS, Q Exactive, Thermo Fisher Scientific, Waltham, MA). A 2 μL sample was loaded onto a Hypersil Gold column (particle size 1.9 μm, 2.1 × 100 mm, Thermo Fisher Scientific) and eluted at 0.30 mL/min with water (A) and methanol (B), each containing 10 mM ammonium acetate. The linear gradient was 95% A for 0 to 1 min, 5% A for 6 to 8 min, and 95% A for 8 to 10 min. Samples were analyzed by a full scan (m/z 50 to 750) at a resolution of 140,000 (m/z 200) under the negative electrospray ionization mode. The suspect and nontarget screening procedure was described in *SI Appendix*, *Supplemental Methods*.

16S rRNA Gene Amplicon Sequencing Analysis. Genomic DNA was extracted from the biomass growing in suspension and attached to the cathode material in both the bioelectrochemical and biological systems. The DNA samples were sent to Laragen (Culver, CA) for 16S rRNA gene amplicon sequencing using MiSeq PE250. The primers targeting the V3–4 region of the 16S rRNA gene were used, i.e., forward primer 5′-CCTACGGGNGGCWGCAG and reverse primer 5′-GACTACHVGGGTATCTAATCC. Sequences were analyzed on the microbiome bioinformatics platform QIIME 2 v2022.2 (https://qiime2.org/). Raw sequences (45) were first imported into QIIME 2 and subject to assembly, quality control (with a minimum quality score of 25), and feature table construction using DADA2. The obtained amplicon sequencing variances were further clustered into operational taxonomic units (OTUs) with a minimum of 99% similarity. The most abundant sequence was automatically selected as the representative sequence for each specific OTU. The closest taxonomy (TAXA) at the genus level was assigned to each OTU using gg-13-8-99-515-806-nb-classifier. Each TAXA may contain multiple OTUs (*SI Appendix*, Table S2 and Fig. S6) due to the low resolution of the taxonomic level.

Data, Materials, and Software Availability. The 16S rRNA amplicon sequencing raw reads were deposited to the National Center for Biotechnology Information (NCBI) BioProject (https://www.ncbi.nlm.nih.gov/bioproject) under the accession number PRJNA913546. All other data are included in the manuscript and/or *SI Appendix*.

ACKNOWLEDGMENTS. This study was supported by the National Institute of Environmental Health Sciences (Award No. R01ES032668, for S.C., X.G., R.R., C.L., and Y.M.) and Strategic Environmental Research and Development (Project No. ER20-1541, for Y.Y. and Y.M.).

1. D. K. Dogutan, D. G. Nocera, Artificial photosynthesis at efficiencies greatly exceeding that of natural photosynthesis. *Acc. Chem. Res.* **52**, 3143–3148 (2019), 10.1021/acs.accounts.9b00380.
2. N. Kornienko, J. Z. Zhang, K. K. Sakimoto, P. Yang, E. Reisner, Interfacing nature's catalytic machinery with synthetic materials for semi-artificial photosynthesis. *Nat. Nanotechnol.* **13**, 890–899 (2018).
3. K. K. Sakimoto, N. Kornienko, P. Yang, Cyborgian material design for solar fuel production: The emerging photosynthetic biohybrid systems. *Acc. Chem. Res.* **50**, 476–481 (2017).
4. H. Chen, F. Dong, S. D. Minteer, The progress and outlook of bioelectrocatalysis for the production of chemicals, fuels and materials. *Nat. Catal.* **3**, 225–244 (2020).
5. T. Zhang, More efficient together. *Science* **350**, 738–739 (2015).
6. S. Cestellos-Blanco, H. Zhang, J. M. Kim, Y.-X. Shen, P. Yang, Photosynthetic semiconductor biohybrids for solar-driven biocatalysis. *Nat. Catal.* **3**, 245–255 (2020).
7. K. P. Nevin, T. L. Woodard, A. E. Franks, Z. M. Summers, D. R. Lovley, Microbial electrosynthesis: Feeding microbes electricity to convert carbon dioxide and water to multicarbon extracellular organic compounds. *mBio* **1**, e00103-10 (2010).
8. C. Liu, B. C. Colón, M. Ziesack, P. A. Silver, D. G. Nocera, Water splitting-biosynthetic system with CO_2 reduction efficiencies exceeding photosynthesis. *Science* **352**, 1210–1213 (2016).
9. C. Liu, K. K. Sakimoto, B. C. Colón, P. A. Silver, D. G. Nocera, Ambient nitrogen reduction cycle using a hybrid inorganic–biological system. *Proc. Natl. Acad. Sci. U.S.A.* **114**, 6450–6455 (2017).
10. R. M. Rodrigues *et al.*, Perfluorocarbon nanoemulsion promotes the delivery of reducing equivalents for electricity-driven microbial CO_2 reduction. *Nat. Catal.* **2**, 407–414 (2019).
11. S. Lu, X. Guan, C. Liu, Electricity-powered artificial root nodule. *Nat. Commun.* **11**, 1505 (2020).
12. X. Guan *et al.*, Maximizing light-driven CO_2 and N_2 fixations in biology-material hybrids. *Nat. Catal.* **5**, 1019–1029 (2022).
13. S. J. Barnabas *et al.*, Extraction of chemical structures from literature and patent documents using open access chemistry toolkits: A case study with PFAS. *Digital Discovery* **1**, 490–501 (2022), 10.1039/D2DD00019A.
14. M. G. Evich *et al.*, Per- and polyfluoroalkyl substances in the environment. *Science* **375**, eabg9065 (2022).
15. Z. Y. Wang, J. DeWitt, C. P. Higgins, I. T. Cousins, A never-ending story of per- and polyfluoroalkyl substances (PFASs)? *Environ. Sci. Technol.* **52**, 3325–3325 (2018).
16. J. Gluge *et al.*, An overview of the uses of per- and polyfluoroalkyl substances (PFAS). *Environ. Sci.: Process. Impacts* **22**, 2345–2373 (2020).
17. C. J. Young *et al.*, Perfluorinated acids in Arctic snow: New evidence for atmospheric formation. *Environ. Sci. Technol.* **41**, 3455–3461 (2007).
18. F. Xiao, Emerging poly- and perfluoroalkyl substances in the aquatic environment: A review of current literature. *Water Res.* **124**, 482–495 (2017).
19. K. Rankin, S. A. Mabury, T. M. Jenkins, J. W. Washington, A North American and global survey of perfluoroalkyl substances in surface soils: Distribution patterns and mode of occurrence. *Chemosphere* **161**, 333–341 (2016).
20. J. Liu, S. Mejia Avendano, Microbial degradation of polyfluoroalkyl chemicals in the environment: A review. *Environ. Int.* **61**, 98–114 (2013).
21. S. Che *et al.*, Structure-specific aerobic defluorination of short-chain fluorinated carboxylic acids by activated sludge communities. *Environ. Sci. Technol. Lett.* **8**, 668–674 (2021).
22. B. Jin *et al.*, Aerobic biotransformation and defluorination of fluoroalkylether substances (ether PFAS): Substrate specificity, pathways, and applications. *Environ. Sci. Technol. Lett.* **10**, 755–761 (2023), 10.1021/acs.estlett.3c00411.
23. L. P. Wackett, Nothing lasts forever: Understanding microbial biodegradation of polyfluorinated compounds and perfluorinated alkyl substances. *Microb. Biotechnol.* **15**, 773–792 (2022).
24. Y. Yu *et al.*, Microbial defluorination of unsaturated per- and polyfluorinated carboxylic acids under anaerobic and aerobic conditions: A structure specificity study. *Environ. Sci. Technol.* **56**, 4894–4904 (2022).
25. P. L. McCarty, C. S. Criddle, T. M. Vogel, Retrospective on microbial transformations of halogenated organics. *Environ. Sci.: Process. Impacts* **22**, 512–517 (2020).
26. R. Zhang *et al.*, Proteomic and metabolic elucidation of solar-powered biomanufacturing by bio-abiotic hybrid system. *Chem* **6**, 234–249 (2020).
27. Y. Yu *et al.*, Microbial cleavage of C–F bonds in two C6 per- and polyfluorinated compounds via reductive defluorination. *Environ. Sci. Technol.* **54**, 14393–14402 (2020).
28. Y. Yu *et al.*, Electron bifurcation and fluoride efflux systems implicated in defluorination of perfluorinated unsaturated carboxylic acids by *Acetobacterium* spp. *Sci. Adv.*, in press.
29. D. A. Lutterman, Y. Surendranath, D. G. Nocera, A self-healing oxygen-evolving catalyst. *J. Am. Chem. Soc.* **131**, 3838–3839 (2009).
30. E. L. Schymanski *et al.*, Identifying small molecules via high resolution mass spectrometry: Communicating confidence. *Environ. Sci. Technol.* **48**, 2097–2098 (2014).
31. L. Schwab, L. Rago, C. Koch, F. Harnisch, Identification of *Clostridium cochlearium* as an electroactive microorganism from the mouse gut microbiome. *Bioelectrochemistry* **130**, 107334 (2019).
32. H. S. Park *et al.*, A novel electrochemically active and Fe (III)-reducing bacterium phylogenetically related to *Clostridium butyricum* isolated from a microbial fuel cell. *Anaerobe* **7**, 297–306 (2001).
33. K. P. Nevin *et al.*, Electrosynthesis of organic compounds from carbon dioxide is catalyzed by a diversity of acetogenic microorganisms. *Appl. Environ. Microbiol.* **77**, 2882–2886 (2011).
34. D. M. J. Shaw *et al.*, Degradation and defluorination of 6:2 fluorotelomer sulfonamidoalkyl betaine and 6:2 fluorotelomer sulfonate by *Gordonia* sp. strain NB4-1Y under sulfur-limiting conditions. *Sci. Total Environ.* **647**, 690–698 (2019).
35. L. P. Wackett, Why is the biodegradation of polyfluorinated compounds so rare? *mSphere* **6**, e0072121 (2021), 10.1128/msphere.00721-00721.
36. S.-H. Yang, Y. Shi, M. Strynar, K.-H. Chu, Desulfonation and defluorination of 6:2 fluorotelomer sulfonic acid (6:2 FTSA) by *Rhodococcus jostii* RHA1: Carbon and sulfur sources, enzymes, and pathways. *J. Hazard. Mater.* **423**, 127052 (2022).
37. S. Joudan, S. A. Mabury, Aerobic biotransformation of a novel highly functionalized polyfluoroether-based surfactant using activated sludge from a wastewater treatment plant. *Environ. Sci.: Process. Impacts* **24**, 62–71 (2022).
38. M. H. Kim, N. Wang, K. H. Chu, 6:2 Fluorotelomer alcohol (6:2 FTOH) biodegradation by multiple microbial species under different physiological conditions. *Appl. Microbiol. Biotechnol.* **98**, 1831–1840 (2014).
39. J. Glüge *et al.*, An overview of the uses of per- and polyfluoroalkyl substances (PFAS). *Environ. Sci.: Process. Impacts* **22**, 2345–2373 (2020).
40. I. Zabaleta *et al.*, Screening and identification of per- and polyfluoroalkyl substances in microwave popcorn bags. *Food Chem.* **230**, 497–506 (2017).
41. T. Okazoe, Overview on the history of organofluorine chemistry from the viewpoint of material industry. *Proc. Jpn. Acad. Ser. B Phys. Biol. Sci.* **85**, 276–289 (2009).
42. G. G. Furin, Perfluorinated carboxylic acids. Synthesis and application. *Fluorine Notes* **5**, 1–2 (2004).
43. Y. J. Men *et al.*, Sustainable syntrophic growth of *Dehalococcoides ethenogenes* strain 195 with Desulfovibrio vulgaris Hildenborough and Methanobacterium congolense: Global transcriptomic and proteomic analyses. *ISME J.* **6**, 410–421 (2012).
44. J. He, V. F. Holmes, P. K. Lee, L. Alvarez-Cohen, Influence of vitamin B_{12} and cocultures on the growth of *Dehalococcoides* isolates in defined medium. *Appl. Environ. Microbiol.* **73**, 2847–2853 (2007).
45. S. Che *et al.*, 16S rRNA gene sequence of bioelectrochemical system. National Center for Biotechnology Information (NCBI) BioProject. https://www.ncbi.nlm.nih.gov/bioproject?term=PRJNA913546. Deposited 18 December 2022.